3D printing of a biocompatible low molecular weight supramolecular hydrogel by dimethylsulfoxide water solvent exchange

Anaïs Chalard, Morgane Mauduit, Sandrine Assié-Souleille, Pierre Joseph, Laurent Malaquin, Juliette Fitremann

3D printing of a biocompatible low molecular weight supramolecular hydrogel by dimethylsulfoxide water solvent exchange

Anaïs Chalard[a,b], Morgane Mauduit[b], Sandrine Souleille[b], Pierre Joseph[b], Laurent Malaquin[b], Juliette Fitremann[a]*

Affiliations

a Laboratoire des IMRCP, Université de Toulouse, CNRS UMR 5623, Université Toulouse III - Paul Sabatier, Toulouse, France

b LAAS-CNRS, Université de Toulouse, CNRS, UPS, Toulouse, France

Keywords: 3D printing; 3D bioprinting; material extrusion, hydrogel; supramolecular; self-assembly; low molecular weight gel; LMWG; self-assembled fibrillar network; SAFIN; fiber; wet spinning, solvent exchange; diffusion; coagulation; carbohydrate; sugar; saccharide; amphiphile; N-alkyl aldonamide; N-heptyl-D-galactonamide

Graphical abstract

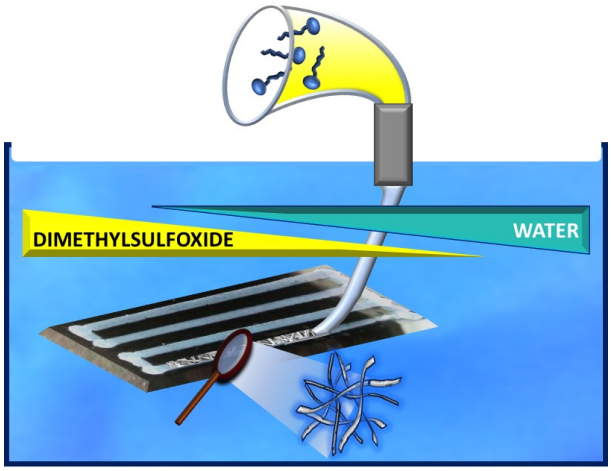

Abstract

A fragile and non-thixotropic biocompatible low molecular weight gel is printed in 3D structures by a solvent exchange process. The 3D printing process is based on the continuous extrusion of a solution of a small amphiphile molecule, N-heptyl-D-galactonamide, in dimethylsulfoxide, that forms a gel in contact with water. The diffusion of water in the dimethylsulfoxide / N-heptyl-D-galactonamide solution triggers the self-assembly of the molecule into supramolecular fibers and the setting of the ink. The conditions for getting a well-defined pattern and the dimensions of the constructs have been determined. The resulting constructs can be easily dissolved, orienting its application as a sacrificial ink or a temporary support. This method opens the way to the injection and the 3D printing of other fragile and non-thixotropic supramolecular hydrogels.

Introduction

3D bioprinting is gaining considerable interest in all fields, from everyday life to cutting edges research[1]. In the context of tissue engineering, it offers a huge potential for designing microenvironments with a high spatial precision and for spatially organizing different populations of cells in the scaffold in a well-controlled manner[2–5]. Bioprinting allows for an accurate control of the architecture, geometry and porosity of scaffolds, especially with synthetic inks and 3D photolithography processes. However, in the context of cell culture applications, the properties of the printed material at the microscopic level are also important since they strongly affect the cell growth and the clearance of the biomaterial[6]. Notably the rigidity, the surface properties, the chemical/biochemical composition, the permeability to cells and the degradability are critical factors controlling cell fate and tissue homeostasis. For this reason, hydrogels are among the best candidates as inks for printing 3D scaffolds for cell culture[7–13].

The techniques for hydrogel 3D printing are primarily based on inkjet droplet deposition, photo-crosslinking, fused deposition (melted ink followed by cooling)[14], thixotropy (decrease of the viscosity under shear, then increase of the viscosity at rest, after injection)[15–20], extrusion of a viscous fluid followed by post-reaction. In all these techniques the injection is made in air. An alternative technique referred as wet spinning relies on the fast setting of an ink of low viscosity in a liquid coagulation bath[21]. This technique is the closest to what we describe here. Nearly all 3D printed hydrogel architectures are based on highly cross-linked polymers, leading to a dense hydrogel. By contrast, still keeping in mind

the potential interactions with cells, we set ourselves the challenge of 3D printing architectures with an extremely low density, soft and delicate hydrogel based on a single small molecule, the N-heptyl-D-galactonamide. This very simple molecule forms a supramolecular hydrogel at concentrations below 0.5 wt%. This kind of hydrogels, called low molecular weight hydrogels (LMWG) or molecular hydrogels are based on the self-assembly of small gelling molecules by non-covalent interactions into a network of fibers or ribbons that entraps water[22–32]. Since they are only formed by small molecules and weak interactions, they give rise to soft hydrogels, suitable for the culture of some types of cells requiring very soft matrices such as neurons. They are also expected to be more permeable to cells facilitating the growth in 3D. In addition, in the context of 3D printing, they are much easier to dissolve, and thus, to remove, compared with polymers, by applying the right washing conditions. As such, they could be used as sacrificial or fugitive inks[33]. 3D printed architectures made of hydrogels that are not based on polymers but based on small gelling molecules are still scarcely described in literature[23,34–39] and most of them are based on self-assembling gelling peptides. In these examples, extrusion printing relies on the thixotropy and/or in-, on post-process gelation (typically, the change of pH after extrusion leads to the gelation of the gelling peptides) or on electrostatic self-assembly similar to the layer-by-layer technique[38]. However, in most of those examples involving molecular hydrogels, the ink is a mixture of the molecular gel and a polymer in order to improve the printability and the resolution of the 3D printed architecture. This strategy mixes the properties of polymer gels and molecular gels[36].

In our preceding work, we showed that low molecular weight hydrogels of N-alkylglyconamides and more especially, N-heptyl-D-galactonamide (GalC7), are biocompatible and allow the growth and the differentiation of human neural stem cells into neurons and glial cells[40]. For different applications, we were looking for methods that would enable to inject or extrude those gels. These hydrogels are prepared by slowly cooling an aqueous solution of the N-heptyl-D-galactonamide and are not thixotropic: upon extrusion, the gels just pack and expulse water and cannot recover their shape. The thermal method was also excluded: the gelling point of a solution of N-heptyl-D-galactonamide is around 90°C which precludes a practical use in 3D printing. However, we further demonstrated that the injection at room temperature of a solution of N-heptyl-D-galactonamide in dimethylsulfoxide (DMSO) in a bath of water triggers the self-assembly of the molecule into a continuous filament of gel[41]. In addition to triggering the formation of the gel, it enables a very good control of the self-assembly mechanism, what was shown in other works[24,25,42]. This result prompted us to adapt this method to 3D printing. With this technique, a very fast gelation occurs by solvent exchange. It ensures the deposition of pretty well-defined patterns over several layers. The resulting construct is thus made only of N-heptyl-D-galactonamide and water. This technique could be a more generic method, adaptable to a large number of small gelling molecules or polymers. We have shown previously that since the DMSO is highly diluted in the water bath, its concentration in the hydrogel is below the detection limits, even a short time after the gel formation. As a consequence, cells can be grown on the gel resulting from this process, opening perspectives for its use in cell culture scaffolds[41].

Experimental Part

3D printing set up

The 3D printing device (see Figure SI-1) consists of a syringe pump (CETONI NEMESYS 290N) controlled by the neMESYS User Interface software) and an XY-translation stage (Newport Universal Motion Controller / Driver, model ESP300, controlled by a Labview interface). The translation stage is programmed to run at different velocities (from 2 to 6 mm/s). A blunt-tip needle (gauge: 22G or 23G) is attached via an arm to a handheld Z-adjustable platform, itself fixed to the XY moving stage. Changes in Z are monitored out manually using a vernier mounted on the moving stage. The syringe was

connected to the needle with a flexible tube. The GalC7 / DMSO solution is extruded at room temperature (between 21 and 23 °C) into a water bath placed on a static stage. The needle extremity was plunged into the water bath. The distance between the glass and the needle was set between 0.5 and 5 mm.

The extrusion flow rate of the GalC7 / DMSO solution is controlled by the syringe pump. With the program used, changes in direction in X or Y are made with 1.15 seconds of latency during which the flow of the GalC7 / DMSO solution is not stopped. The ultrapure water bath is made in a Petri dish (10 cm diameter) filled with 7.5mL of DI water height. The Petri dish is fixed by an adhesive to the static stage. At the bottom of the water bath is placed a glass slide covered with a hydrophobic polycarbonate membrane (it4ip ipPORE track etched membrane, 21 µm thick, pore diameter of 5 µm, pore density of 10^5 cm^{-2}), attached with an adhesive tape.

Gelling solution

Solutions of *N*-heptyl-D-galactonamide in dimethylsulfoxide are prepared by dissolving the powder at 2.5 wt% (25 mg/mL) at room temperature with the help of an ultrasound bath. The synthesis of *N*-heptyl-D-galactonamide has been described elsewhere[40] or it can be purchased from Innov'Orga, Reims, France. Dimethylsulfoxide has been purchased from Fisher, quality 99 %, non-anhydrous.

Measurement of the width of the printed deposit by optical microscopy

The widths of the deposits are measured out of optical microscopy observations. After printing the gels, the glass slide covered with the membrane is taken out of the water bath and rapidly observed with an inverted optical microscope (Olympus, bright field, ×4 or ×10 objectives). The widths are measured with ImageJ software at different places of the deposit and the mean width as well as the standard deviation are calculated. The results of these measurements are given in SI-2.

Determination of the profile of the printed deposit

Two methods are used. After printing, the glass slide is placed on a water-soaked paper inside a Petri dish and observed with microscope. The glass slide / polycarbonate membrane and the gel are kept on the soaked paper throughout the whole observation. The first microscope used is a Hirox (Hirox HI-SCOPE advanced KH-3000, CT-7 motor controller) with an electronic Z stage. To get the profiles of the deposits, the focus is first made on the polycarbonate membrane and the sample was moved perpendicularly to the direction of the deposit. The focus was adjusted every 50 µm and the displacement in Z was measured along the section. The Z displacement was plotted against the X displacement, giving the profile of the gel. The second microscope used is a Keyence optical numeric microscope (model VHX-1000). This microscope has an integrated software that automatically focuses and detects the profile of the gel deposits.

Cryo-SEM microscopy

After printing the gel, the glass slide / polycarbonate membrane set is taken out of the bath and kept in a humid sealed Petri dish for transportation to the electronic microscopy facilities. A sample of the polycarbonate membrane with the hydrogel is cut and is deposited on the cryo-SEM cane and frozen at −220 °C in liquid nitrogen. The frozen sample was put at −145 °C under vacuum in the cryo-transfer system chamber (Quorum PP3000T) without fracturing (the polycarbonate membrane is not rigid enough). The freeze-drying was performed at −95 °C for 30 min. The sample was metalized with Pd for 60 s and introduced in the microscope chamber. The temperature was kept at −145 °C. Images were recorded with a FEG FEI Quanta 250 microscope, at 5 kV for the acceleration voltage.

Results and Discussion

Principle

The method used for printing the LMWG GalC7 in 3D is based on the fast gelation of a solution GalC7/dimethylsulfoxide (DMSO) in contact with water (Figure 1). Typically, a solution of GalC7 at 2.5 wt% in DMSO is injected with a blunt-tip needle (23G) in a bath of water. The extremity of the needle is immersed in the bath. GalC7 has a poor solubility in water and the diffusion of the water inside the DMSO jet triggers its self-assembly into supramolecular fibers. The patterns are drawn by moving the nozzle in X, Y and Z in a static bath of water. We have previously evidenced that during the injection of a GalC7/DMSO jet in a bath of water the gelation is fast enough and occurs during the DMSO fall. This mechanism allows for the formation of a continuous filament of gel. This method is known for polymers as "wet spinning"[41]. In this technique, the gelation progressively occurs in the jet during its fall away from the nozzle exit, driven by water and DMSO mutual diffusion. The residence time in water needs to be long enough to allow the diffusion of water to trigger the self-assembly, at least at the surface of the jet. However, in order to guaranty the construction of 3D architecture, the gelation process should be not be completed so that the filament is capable to adhere to the surface or to the previously assembled structures. Following this idea, we quantified the main conditions that need to be met to obtain a stable printing process and we compared it with our experimental observations.

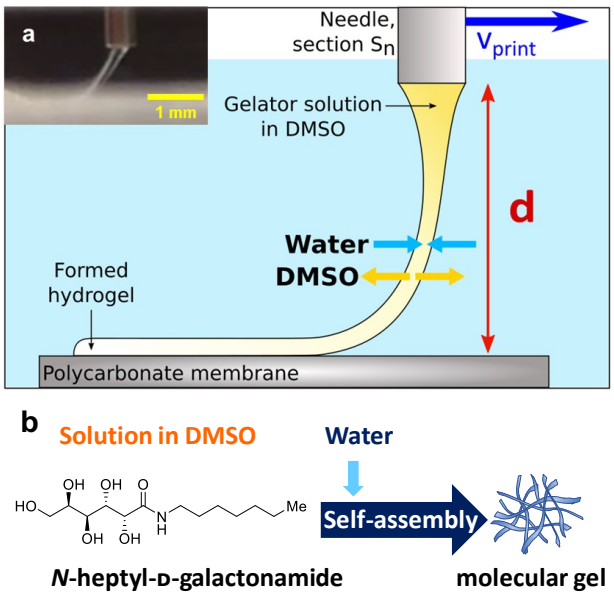

Figure 1: *a. Principle of 3D printing of N-heptyl-D-galactonamide (GalC7) by solvent exchange. Blue arrow: printing speed. Red arrow: distance needle to polycarbonate membrane. Inserted (top left): Observation of the DMSO jet after the needle exit during the printing (extrusion rate of 10 µl/min, printing speed of 3 mm/s, 23G needle, GalC7 concentration 2.5 wt% in DMSO). b. structure of GalC7 and self-assembly mechanism.*

Adhesion

Promoting hydrogel adhesion on the surface on which it is printed is a critical factor in the 3D printing process. First, we investigated the adhesion capabilities of various substrate materials. On glass, the adhesion was poor whatever the flow rate or needle/substrate distance. Conversely, the printing on a polycarbonate membrane gave positive results and allowed for the adhesion of the first layer in some conditions. We observed that moving the nozzle closer to the deposition surface, in addition to enabling a higher precision of deposition, improved significantly the adhesion. These observations, as well as the influence of the printing speed (v_{print}) are shown in Figure 2. Interestingly increasing the writing speed or increasing the nozzle-surface distance d resulted in a decrease of the adhesion properties. We analyze these results by defining simple process criteria: the GalC7 solution needs to be deposited as a non-fully gelled filament for a proper deposition. This condition can be expressed by stating that the time left to the jet to reach the surface (τ_{fall}) should be shorter than the typical gelation time τ_{gel}. As discussed in our work on wet spinning[41], gelation of a filament is typically controlled by mutual diffusion of water and DMSO from the shell to the core of the jet. A filament with section S_f thus gelifies within a typical time of order $\tau_{gel} \cong S_f/D_{eff}$, where D_{eff} is an effective diffusion coefficient accounting for water and DMSO exchange. Since adhesion implies no slip of the filament with respect to the surface, the filament volume per time unit is equal to $S_f.v_{print}$. It is set by the syringe flow rate Q_{eject} : $S_f.v_{print} = \alpha.Q_{eject}$, where α is a unitless constant with an order of magnitude of 1 (α reflects the volume change during the water-DMSO exchange: with no volume variation, α would be equal to 1. In the case of DMSO/water exchange, the volume is not exactly conserved, see ref[41]). In this qualitative model, we estimated the falling time τ_{fall} from the initial mean fluid velocity at the exit of the syringe $v_{eject} = Q_{eject}/S_n$ (with S_n the syringe needle section), since the printing process mainly affects the horizontal velocity. It gives: $\tau_{fall} \sim d/v_{eject} = d.S_n/Q_{eject}$.
The adhesion condition can thus be written $\tau_{fall} \leq \beta\, \tau_{gel}$, where β is a unitless constant that characterizes the rate of gelling in the filament. By combining the previous consideration to express the filament section as function of process parameters, the adhesion criteria gives:

$$d.\frac{S_n}{Q_{eject}} \leq \beta \frac{\alpha.Q_{eject}}{v_{print}.D_{eff}}$$

Which finally leads to the condition:

$$d.v_{print} \leq \frac{\alpha\,\beta\,Q_{eject}^2}{D_{eff}.S_n} \qquad (1)$$

For fixed flow rate and needle gauge, this prediction is fully consistent with the process diagram shown in Figure 2a: needle-surface distance d needs to be short enough and v_{print} small enough, to ensure correct attachment of the filament of the substrate. Even though our analysis is not quantitative, it is worth noting that Equation (1) leads to very reasonable estimates for the transition between correct and non-correct adhesion, either for a 23G or for a 22G nozzle gauge. For example, with Q_{eject} = 5 µL/min for a 23G nozzle (~~needle~~ internal diameter 0.34 mm, S_n = 0.09 mm^2) the ejection velocity is v_{eject} = 0.9 mm/s. For a printing velocity v_{print} = 6 mm/s, α = 1 and with the value $D_{eff} \sim 0.9.10^{-9}$ m^2/s ([43]), Equation (1) leads to a predicted maximal value of the needle-substrate distance: $d_{max} \cong 14$ mm, by setting β = 1. This value of β = 1 corresponds to a full gelation of the filament over its whole thickness. However, the adhesion diagram in Figure 2a shows that adhesion is good up to a maximum value of 2 mm, in the same conditions (v_{print} = 6 mm/s, flow rate = 5 µL/min, 23G needle). By setting β = 0.14 instead of β = 1, a curved line can be drawn from Equation 1 and is reported on Figure 2a (the dash blue line). This curve fits quite well with the experimental results by separating adhesion and non-adhesion conditions. Except for two points, the experimental points are well classified by the model: points below the curve correspond to good adhesion, as opposed to conditions above the curve: too high velocity or distance prevents adhesion for most measurements. It can be understood as follows: the actual process criteria (good adhesion / no adhesion) does not require full gelation. At the limit,

the outer shell of the filament is already gelled, but not the inside of the filament. The model thus shows that a fraction of the gelled shell is sufficient to impair adhesion.

Interestingly, this analysis also nicely captures the influence of the different process parameters, in addition to that of the printing speed and needle-substrate distance already discussed. The flow rate strongly affects adhesion (square dependence) according to two cumulating mechanisms: increasing Q_{eject} increases the filament section, leading to longer gelation time and it reduces the flight time to reach the substrate. Accordingly, this adhesion favoured by high flow rate is observed for both needle gauges 23G (Figure 2a, top) and 22G (Figure 2a, below).

Additional trials were performed to assess the influence of the concentration. With a more concentrated solution (4 wt% instead of 2.5 wt%), the adhesion is lower, because of quicker gelation.

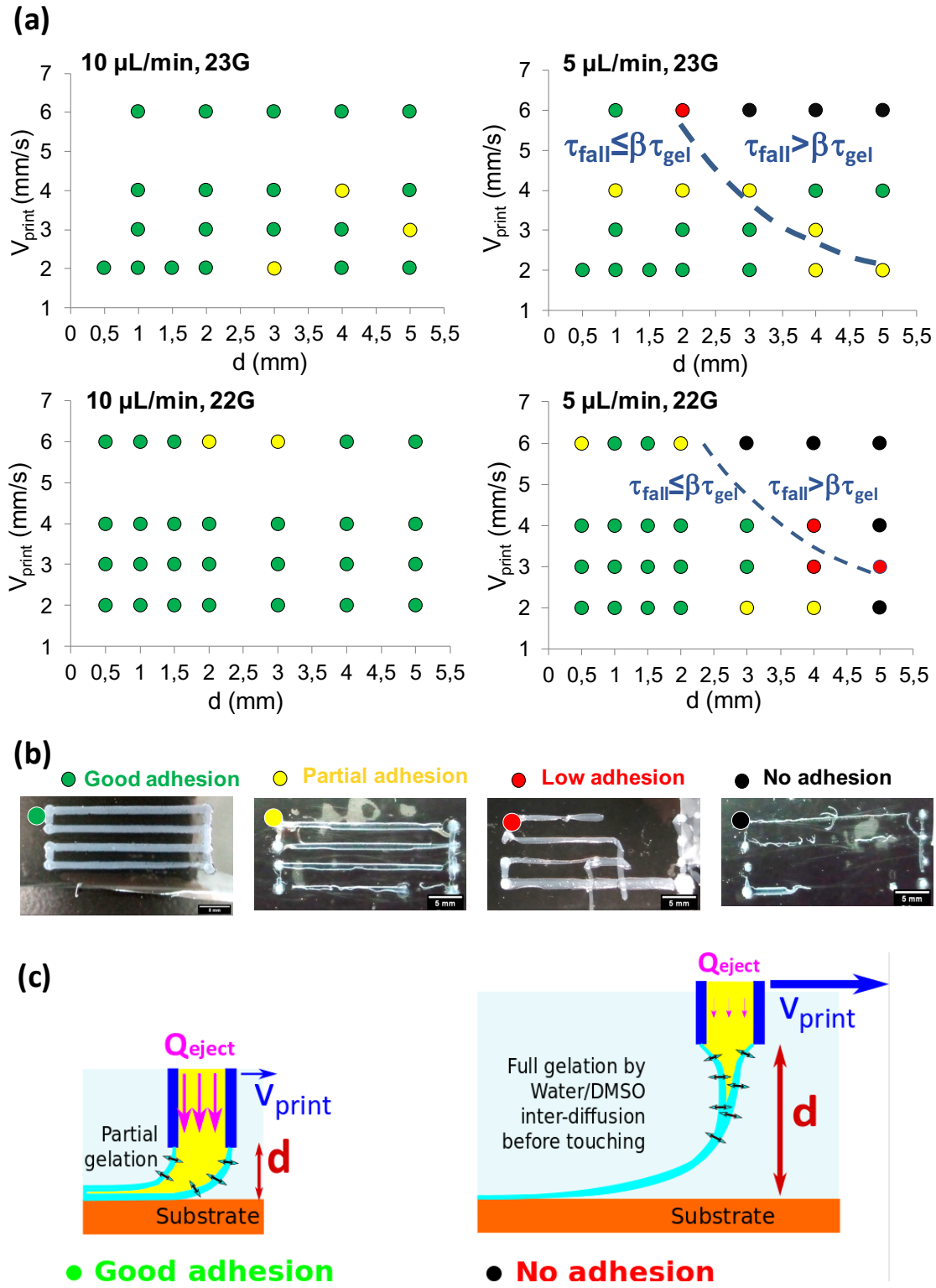

Figure 2: *(a) Adhesion phase diagrams at two flow rates (10 µL/min and 5 µL/min), and with two nozzle gauges (23G and 22G) as a function of the printing speed (v_{print}) and the distance "d" between the needle and the deposition membrane. Concentration of N-heptyl-D-galactonamide in DMSO = 2.5 wt%. The dashed blue line is the model prediction for the transition between adhesive and non-adhesive conditions, with β = 0.14. (b) Pictures of the resulting 3D printed patterns in the different conditions (scale bar: 5 mm). (c) Scheme of the mechanisms controlling the process: sufficiently high flow rate, low printing velocity and short needle-substrate distance allow an incomplete gelation and favour adhesion of the filament on the substrate.*

In summary, all these results lead to the same conclusion, schematically summarized in Figure 2c: if the solution is already gelled (longer residence time in water because of low flow rate or large needle-substrate distance, higher concentration, thinner nozzle), the adhesion is not good. Finally, the following conditions were used for the rest of the study: concentration 2.5 wt%, needle-membrane distance 2mm, needle diameter 22G or 23G, injection flow rate 10 µL/min and 5 µL/min.

Profiles of the printed structures

The profiles of the printed hydrogel have been studied in different conditions of needle size (22G and 23G), injection flow rate (5 µL/min and 10 µL/min) and printing speed (2, 3, 4, 6 mm/s). They have been recorded with two different microscopes equipped with a motorized Z stage, but with a manual (Hirox) or automated (Keyence) focus according to Z. The corresponding profiles are given in Figure 3 and in SI-2. The widths of the deposits only (not the heights) have been also measured by standard optical microscopy and are reported in SI-3. The deposited filaments are wider than their height, due to the good wetting of the polycarbonate substrate. In addition, the falling gel is mostly cylindrical (which controls the initial adhesion, as already described) and because it is only partially gelled when it contacts the substrate, it adopts a flat shape. Accordingly, the filament section is completely consistent with the value deduced from the flow rate. Taking the same numerical example as before (23G, 5µL/mn, 6mm/s), the experimental value of the section in the case of a deposited filament, determined from Figure 3a is S_{exp} ~ 35 x 500 µm^2 = 0.017 mm^2 (width x height of the deposit). This value is very similar to the one computed from the flow rate, $S_f = \alpha . Q_{eject}/v_{print} \approx$ 0.014 mm^2 (considering α = 1), especially considering that volume is not exactly preserved due to solvent exchange (water-DMSO). The effect of the printing speed and the flow rate (Figures 3, SI-2 and SI-3) is also consistent with the model presented in the previous paragraph: by increasing the printing speed or by decreasing the injection flow rate, the volume of gel deposited per unit length of the substrate is smaller, resulting in the decrease of the deposit width and height. The profile of two successive layers has been recorded (Figure 3b). The maximal heights of the cross sections are the following: 50 µm for the first layer and 130 µm for the second one. It shows that the additive process takes place conveniently without collapsing the lower layer neither enlarging too much the deposit. Finally, 15 successive layers have been printed, providing the 3D architecture of 9 squares in Figure 3c. The setting of the gel is fast enough to reproduce with a quite good fidelity all the right angles of the designed pattern. Compared to a 3D printing of hydrogels relying on thixotropy, the spreading of the ink is much reduced. At this stage of the study, we used a home-made 3D printer that stops for 1.15 s at each change of direction and between two layers. Meanwhile the flow of the gelling solution does not stop, so it delivers an extra 0.2 µL of the gelling solution at each corner, leading to the enlargement of the structure at these places. This point should be improved with a more advanced 3D printer. It could be compensated by appropriately tuning the acceleration to keep the linear velocity constant during the whole printing process. The microstructure of the gel has been observed by cryo-SEM. The supramolecular fibers are quite homogeneous in size with a fiber width around 235 nm (Figure 3d). Finally, an important fact has to be pointed out here for the practical use of the N-heptyl-D-galactonamide 3D printed gel. With this molecule, the supramolecular fibers tend to dissolve quite quickly, within few hours, if the printed structure is kept in the large volume of water used during the 3D printing process (7.5 mL). In order to keep the 3D printed structure longer, the excess water must be removed after printing. A small amount of water can be kept in the squares to keep the structure hydrated. This property makes this hydrogel a good candidate for using it as a sacrificial ink. Alternatively, to get more durable architectures, this method has to be adapted to less soluble gelators.

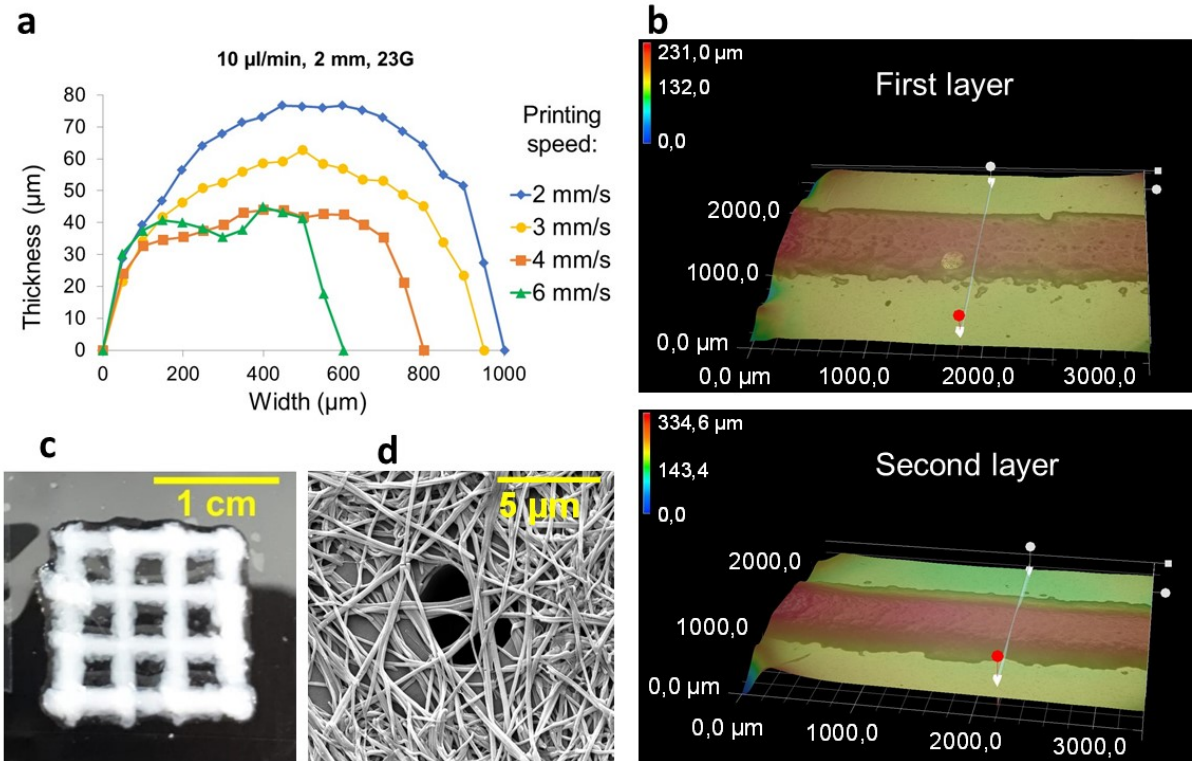

Figure 3: *(a) Printed deposits' profiles at different printing speeds (Hirox microscope). (b) Profilometry analysis of the deposits with the Keyence microscope (V_{print} = 3 mm/s). (c). Photo of a 3D printed hydrogel scaffold obtained after 15 additive layers. The width of the printed structures at the center is around 1.8 mm. (d) cryo-SEM of the first layer. Concentration of N-heptyl-D-galactonamide in DMSO = 2.5 wt%. 23G needle. Extrusion rate Q_{eject}= 10 µl/min. Distance needle/membrane: d = 2 mm.*

Conclusion

The gels of N-heptyl-D-galactonamide are not thixotropic and cannot be extruded once gelled because of their mechanical fragility. An alternative method for 3D printing this hydrogel, based on solvent exchange has been found and is quite easy to implement. In addition, the N-heptyl-D-galactonamide is easy to prepare as a pure molecule without issues related to batch to batch variation that are usually found with polymers. The gels of N-heptyl-D-galactonamide are biocompatible and we have shown that the introduction of DMSO in the process does not impair the cell growth. The DMSO diffuses in the large volume of water and further, it is washed out with culture medium. Despite their low duration in water, these 3D architectures could be incorporated in biocompatible scaffolds, notably as a sacrificial ink. We have also shown in preliminary results that similar molecules, such as N-octyl and N-hexyl-D-galactonamide also self-assemble quickly in wet spinning conditions and form gel filaments. Consequently, this method of 3D printing can be probably adapted to many other LMWG, providing a solution for the 3D printing of non-thixotropic gels. We found that a critical parameter is the speed of gelling in contact with water, which affects the adhesion, the width and the cohesion of the deposited layers. The persistence of the 3D architecture in water is another important point if they have to be used in cell culture experiments. It is affected by the solubility of the gelator in water. Since all LMWG have different solubilities in water and self-assembly properties and energy, exploration of libraries of these molecules is likely to provide 3D architectures with variable resolutions and more or less

persistent in water. They could thus be selected depending on the application. Also, different formulations may be tested to improve the quality of this ink and to extend the scope of the method[44]. The role and the specific qualities of the dimethylsulfoxide as the jet solvent (notably the density, viscosity and initial interfacial tension) still have to be studied for a better understanding of this method.

Author statement

Anaïs Chalard: Conceptualization, Methodology, Investigation, Validation, Writing - Original Draft, Writing - Review & Editing, Vizualisation. **Morgane Mauduit**: Investigation, Methodology, Validation, Writing - Original Draft, Writing - Review & Editing, Vizualisation. **Sandrine Souleille**: Ressources, Software, Investigation. **Pierre Joseph**: Conceptualization, Methodology, Validation, Formal analysis, Supervision, Funding acquisition, Writing - Original Draft, Writing - Review & Editing, Visualization. **Laurent Malaquin**: Conceptualization, Methodology, Validation, Formal analysis, Supervision, Funding acquisition, Writing - Original Draft, Visualization. **Juliette Fitremann**: Conceptualization, Methodology, Investigation, Validation, Supervision, Project administration, Funding acquisition, Writing - Original Draft, Writing - Review & Editing, Visualization.

Acknowledgements

Nathan Trouvain and Chloé Oneda are acknowledged for their assistance in preliminary experiments. We acknowledge CIRIMAT and Vincent Baylac (CIRIMAT, Toulouse) for providing access and for assistance in the recording of 3D profiles with Keyence microscope. Bruno Payré, Isabelle Fourquaux and Dominique Goudounèche (CMEAB, Toulouse) are acknowlegded for their assistance in the acquisition of electronic microscopy images. This work was supported by the French National Research Agency (A.C.'s grant and financial support, ANR "Neuraxe", grant N°ANR-15-CE07-0007-01) and as part of the MultiFAB project which has received funding from FEDER European Regional Funds and Région Occitanie - France (Grant number: 16007407/MP0011594). The European Union is also acknowledged for its financial support for equipment (FEDER-35477: "Nano-objets pour la biotechnologie"). This work was partly supported as part of the the HoliFAB project funded by the European Union's Horizon 2020 research and innovation program (grant agreement No 760927).

Data availability

The raw data are available on request to the corresponding author J.F. It contains the photos of the apparatus used, photos of the printed structures as a function of the printing speed, extrusion rate, needle to membrane distance or needle to glass distance, concentration, needle diameter. From these images, adhesion, clogging and the experimental conditions in which the printing was possible were determined. All raw graphics and tables sorting these data are also available. It contains videos of the 3D printing process. It contains also the digital microscope images providing the width and the height of the printed structures and extra electronic microscopy images of the printed hydrogel.

References

(1) Ligon, S. C.; Liska, R.; Stampfl, J.; Gurr, M.; Mülhaupt, R. Polymers for 3D Printing and Customized Additive Manufacturing. *Chem. Rev.* **2017**, *117* (15), 10212–10290. https://doi.org/10.1021/acs.chemrev.7b00074.

(2) Lee, A.; Hudson, A. R.; Shiwarski, D. J.; Tashman, J. W.; Hinton, T. J.; Yerneni, S.; Bliley, J. M.; Campbell, P. G.; Feinberg, A. W. 3D Bioprinting of Collagen to Rebuild Components of the Human Heart. *Science* **2019**, *365* (6452), 482–487. https://doi.org/10.1126/science.aav9051.
(3) Tappa, K.; Jammalamadaka, U. Novel Biomaterials Used in Medical 3D Printing Techniques. *Journal of Functional Biomaterials* **2018**, *9* (1), 17. https://doi.org/10.3390/jfb9010017.
(4) Ding, S.; Feng, L.; Wu, J.; Zhu, F.; Tan, Z.; Yao, R. Bioprinting of Stem Cells: Interplay of Bioprinting Process, Bioinks, and Stem Cell Properties. *ACS Biomater. Sci. Eng.* **2018**, *4* (9), 3108–3124. https://doi.org/10.1021/acsbiomaterials.8b00399.
(5) Huang, Y.; Zhang, X.-F.; Gao, G.; Yonezawa, T.; Cui, X. 3D Bioprinting and the Current Applications in Tissue Engineering. *Biotechnology Journal* **2017**, *12* (8), 1600734. https://doi.org/10.1002/biot.201600734.
(6) Caliari, S. R.; Burdick, J. A. A Practical Guide to Hydrogels for Cell Culture. *Nat Methods* **2016**, *13* (5), 405–414. https://doi.org/10.1038/nmeth.3839.
(7) Bouguéon, G.; Kauss, T.; Dessane, B.; Barthélémy, P.; Crauste-Manciet, S. Micro- and Nano-Formulations for Bioprinting and Additive Manufacturing. *Drug Discovery Today* **2019**, *24* (1), 163–178. https://doi.org/10.1016/j.drudis.2018.10.013.
(8) Luo, Y.; Wei, X.; Huang, P. 3D Bioprinting of Hydrogel-Based Biomimetic Microenvironments. *Journal of Biomedical Materials Research Part B: Applied Biomaterials* **2019**, *107* (5), 1695–1705. https://doi.org/10.1002/jbm.b.34262.
(9) Lee, J. M.; Yeong, W. Y. Design and Printing Strategies in 3D Bioprinting of Cell-Hydrogels: A Review. *Adv. Healthcare Mater.* **2016**, *5* (22), 2856–2865. https://doi.org/10.1002/adhm.201600435.
(10) Valot, L.; Martinez, J.; Mehdi, A.; Subra, G. Chemical Insights into Bioinks for 3D Printing. *Chem. Soc. Rev.* **2019**, *48* (15), 4049–4086. https://doi.org/10.1039/C7CS00718C.
(11) Heidarian, P.; Kouzani, A. Z.; Kaynak, A.; Paulino, M.; Nasri-Nasrabadi, B. Dynamic Hydrogels and Polymers as Inks for Three-Dimensional Printing. *ACS Biomater. Sci. Eng.* **2019**, *5* (6), 2688–2707. https://doi.org/10.1021/acsbiomaterials.9b00047.
(12) Stanton, M. M.; Samitier, J.; Sánchez, S. Bioprinting of 3D Hydrogels. *Lab Chip* **2015**, *15* (15), 3111–3115. https://doi.org/10.1039/C5LC90069G.
(13) Leijten, J.; Seo, J.; Yue, K.; Trujillo-de Santiago, G.; Tamayol, A.; Ruiz-Esparza, G. U.; Shin, S. R.; Sharifi, R.; Noshadi, I.; Álvarez, M. M.; et al. Spatially and Temporally Controlled Hydrogels for Tissue Engineering. *Materials Science and Engineering: R: Reports* **2017**, *119*, 1–35. https://doi.org/10.1016/j.mser.2017.07.001.
(14) Miller, J. S.; Stevens, K. R.; Yang, M. T.; Baker, B. M.; Nguyen, D.-H. T.; Cohen, D. M.; Toro, E.; Chen, A. A.; Galie, P. A.; Yu, X.; et al. Rapid Casting of Patterned Vascular Networks for Perfusable Engineered Three-Dimensional Tissues. *Nature Materials* **2012**, *11* (9), 768–774. https://doi.org/10.1038/nmat3357.
(15) Wang, L. L.; Highley, C. B.; Yeh, Y.-C.; Galarraga, J. H.; Uman, S.; Burdick, J. A. Three-Dimensional Extrusion Bioprinting of Single- and Double-Network Hydrogels Containing Dynamic Covalent Crosslinks. *Journal of Biomedical Materials Research Part A* **2018**, *106* (4), 865–875. https://doi.org/10.1002/jbm.a.36323.
(16) Highley, C. B.; Rodell, C. B.; Burdick, J. A. Direct 3D Printing of Shear-Thinning Hydrogels into Self-Healing Hydrogels. *Adv. Mater.* **2015**, *27* (34), 5075–5079. https://doi.org/10.1002/adma.201501234.
(17) Latxague, L.; Ramin, M. A.; Appavoo, A.; Berto, P.; Maisani, M.; Ehret, C.; Chassande, O.; Barthélémy, P. Control of Stem-Cell Behavior by Fine Tuning the Supramolecular

Assemblies of Low-Molecular-Weight Gelators. *Angew. Chem. Int. Ed.* **2015**, *54* (15), 4517–4521. https://doi.org/10.1002/anie.201409134.
(18) Skilling, K. J.; Kellam, B.; Ashford, M.; Bradshaw, T. D.; Marlow, M. Developing a Self-Healing Supramolecular Nucleoside Hydrogel. *Soft Matter* **2016**, *12* (43), 8950–8957. https://doi.org/10.1039/C6SM01779G.
(19) Pugliese, R.; Fontana, F.; Marchini, A.; Gelain, F. Branched Peptides Integrate into Self-Assembled Nanostructures and Enhance Biomechanics of Peptidic Hydrogels. *Acta Biomaterialia* **2018**, *66*, 258–271. https://doi.org/10.1016/j.actbio.2017.11.026.
(20) Cigognini, D.; Silva, D.; Paloppi, S.; Gelain, F. Evaluation of Mechanical Properties and Therapeutic Effect of Injectable Self-Assembling Hydrogels for Spinal Cord Injury. *J Biomed Nanotechnol* **2014**, *10* (2), 309–323. https://doi.org/10.1166/jbn.2014.1759.
(21) Costantini, M.; Colosi, C.; Święszkowski, W.; Barbetta, A. Co-Axial Wet-Spinning in 3D Bioprinting: State of the Art and Future Perspective of Microfluidic Integration. *Biofabrication* **2018**, *11* (1), 012001. https://doi.org/10.1088/1758-5090/aae605.
(22) Dang-i, A. Y.; Kousar, A.; Liu, J.; Mukwaya, V.; Zhao, C.; Wang, F.; Hou, L.; Feng, C.-L. Mechanically Stable C2-Phenylalanine Hybrid Hydrogels for Manipulating Cell Adhesion. *ACS Appl. Mater. Interfaces* **2019**, *11* (32), 28657–28664. https://doi.org/10.1021/acsami.9b08655.
(23) Chivers, P. R. A.; Smith, D. K. Shaping and Structuring Supramolecular Gels. *Nat Rev Mater* **2019**, *4* (7), 463–478. https://doi.org/10.1038/s41578-019-0111-6.
(24) Lovrak, M.; Hendriksen, W. E. J.; Maity, C.; Mytnyk, S.; van Steijn, V.; Eelkema, R.; van Esch, J. H. Free-Standing Supramolecular Hydrogel Objects by Reaction-Diffusion. *Nature Communications* **2017**, *8*, 15317. https://doi.org/10.1038/ncomms15317.
(25) Lovrak, M.; Hendriksen, W. E.; Kreutzer, M. T.; Steijn, V. van; Eelkema, R.; Esch, J. H. van. Control over the Formation of Supramolecular Material Objects Using Reaction–Diffusion. *Soft Matter* **2019**, *15* (21), 4276–4283. https://doi.org/10.1039/C8SM02588F.
(26) Baccile, N.; Renterghem, L. V.; Griel, P. L.; Ducouret, G.; Brennich, M.; Cristiglio, V.; Roelants, S. L. K. W.; Soetaert, W. Bio-Based Glyco-Bolaamphiphile Forms a Temperature-Responsive Hydrogel with Tunable Elastic Properties. *Soft Matter* **2018**, *14* (38), 7859–7872. https://doi.org/10.1039/C8SM01167B.
(27) Datta, S.; Bhattacharya, S. Multifarious Facets of Sugar-Derived Molecular Gels: Molecular Features, Mechanisms of Self-Assembly and Emerging Applications. *Chem. Soc. Rev.* **2015**, *44* (15), 5596–5637. https://doi.org/10.1039/C5CS00093A.
(28) Draper, E. R.; Adams, D. J. Low-Molecular-Weight Gels: The State of the Art. *Chem* **2017**, *3* (3), 390–410. https://doi.org/10.1016/j.chempr.2017.07.012.
(29) Amabilino, D. B.; Smith, D. K.; Steed, J. W. Supramolecular Materials. *Chem. Soc. Rev.* **2017**, *46* (9), 2404–2420. https://doi.org/10.1039/C7CS00163K.
(30) Zhou, J.; Li, J.; Du, X.; Xu, B. Supramolecular Biofunctional Materials. *Biomaterials* **2017**, *129*, 1–27. https://doi.org/10.1016/j.biomaterials.2017.03.014.
(31) Du, X.; Zhou, J.; Shi, J.; Xu, B. Supramolecular Hydrogelators and Hydrogels: From Soft Matter to Molecular Biomaterials. *Chemical Reviews* **2015**, *115* (24), 13165–13307. https://doi.org/10.1021/acs.chemrev.5b00299.
(32) Vieira, V. M. P.; Lima, A. C.; de Jong, M.; Smith, D. K. Commercially Relevant Orthogonal Multi-Component Supramolecular Hydrogels for Programmed Cell Growth. *Chemistry – A European Journal* **2018**, *24* (56), 15112–15118. https://doi.org/10.1002/chem.201803292.
(33) O'Bryan, C. S.; Bhattacharjee, T.; Niemi, S. R.; Balachandar, S.; Baldwin, N.; Ellison, S. T.; Taylor, C. R.; Sawyer, W. G.; Angelini, T. E. Three-Dimensional Printing with Sacrificial Materials for Soft Matter Manufacturing. *MRS Bulletin* **2017**, *42* (08), 571–577. https://doi.org/10.1557/mrs.2017.167.

(34) Nolan, M. C.; Caparrós, A. M. F.; Dietrich, B.; Barrow, M.; Cross, E. R.; Bleuel, M.; King, S. M.; Adams, D. J. Optimising Low Molecular Weight Hydrogels for Automated 3D Printing. *Soft Matter* **2017**, *13* (45), 8426–8432. https://doi.org/10.1039/C7SM01694H.
(35) Raphael, B.; Khalil, T.; Workman, V. L.; Smith, A.; Brown, C. P.; Streuli, C.; Saiani, A.; Domingos, M. 3D Cell Bioprinting of Self-Assembling Peptide-Based Hydrogels. *Materials Letters* **2017**, *190*, 103–106. https://doi.org/10.1016/j.matlet.2016.12.127.
(36) Cofiño, C.; Perez-Amodio, S.; Semino, C. E.; Engel, E.; Mateos-Timoneda, M. A. Development of a Self-Assembled Peptide/Methylcellulose-Based Bioink for 3D Bioprinting. *Macromolecular Materials and Engineering 0* (0), 1900353. https://doi.org/10.1002/mame.201900353.
(37) Hedegaard, C. L.; Collin, E. C.; Redondo-Gómez, C.; Nguyen, L. T. H.; Ng, K. W.; Castrejón-Pita, A. A.; Castrejón-Pita, J. R.; Mata, A. Hydrodynamically Guided Hierarchical Self-Assembly of Peptide–Protein Bioinks. *Advanced Functional Materials* **2018**, *28* (16), 1703716. https://doi.org/10.1002/adfm.201703716.
(38) Jian, H.; Wang, M.; Dong, Q.; Li, J.; Wang, A.; Li, X.; Ren, P.; Bai, S. Dipeptide Self-Assembled Hydrogels with Tunable Mechanical Properties and Degradability for 3D Bioprinting. *ACS Applied Materials & Interfaces* **2019**, *11* (50), 46419–46426. https://doi.org/10.1021/acsami.9b13905.
(39) Dessane, B.; Smirani, R.; Bouguéon, G.; Kauss, T.; Ribot, E.; Devillard, R.; Barthélémy, P.; Naveau, A.; Crauste-Manciet, S. Nucleotide Lipid-Based Hydrogel as a New Biomaterial Ink for Biofabrication. *Sci Rep* **2020**, *10* (1), 1–11. https://doi.org/10.1038/s41598-020-59632-w.
(40) Chalard, A.; Vaysse, L.; Joseph, P.; Malaquin, L.; Souleille, S.; Lonetti, B.; Sol, J.-C.; Loubinoux, I.; Fitremann, J. Simple Synthetic Molecular Hydrogels from Self-Assembling Alkylgalactonamides as Scaffold for 3D Neuronal Cell Growth. *ACS Appl. Mater. Interfaces* **2018**, *10* (20), 17004–17017. https://doi.org/10.1021/acsami.8b01365.
(41) Chalard, A.; Joseph, P.; Souleille, S.; Lonetti, B.; Saffon-Merceron, N.; Loubinoux, I.; Vaysse, L.; Malaquin, L.; Fitremann, J. Wet Spinning and Radial Self-Assembly of a Carbohydrate Low Molecular Weight Gelator into Well Organized Hydrogel Filaments. *Nanoscale* **2019**, *11* (32), 15043–15056. https://doi.org/10.1039/C9NR02727K.
(42) Wang, Y.; Qi, W.; Huang, R.; Su, R.; He, Z. Jet Flow Directed Supramolecular Self-Assembly at Aqueous Liquid–Liquid Interface. *RSC Adv.* **2014**, *4* (30), 15340–15347. https://doi.org/10.1039/C3RA47483F.
(43) Tsay, C. S.; McHugh, A. J. A Technique for Rapid Measurement of Diffusion Coefficients. *Ind. Eng. Chem. Res.* **1992**, *31* (1), 449–452. https://doi.org/10.1021/ie00001a063.
(44) Chimene, D.; Kaunas, R.; Gaharwar, A. K. Hydrogel Bioink Reinforcement for Additive Manufacturing: A Focused Review of Emerging Strategies. *Advanced Materials* **2020**, *32* (1), 1902026. https://doi.org/10.1002/adma.201902026.